Journal of Computational Applied Mechanics 2026, 57(1): 41-62

DOI: 10.22059/jcamech.2025.399564.1580

RESEARCH PAPER

Computational Analysis of Natural Convection Heat Transfer in Nanofluids Under a Uniform Magnetic Field Using Levenberg–Marquardt Backpropagation Neural Networks

Muhammad Sulaiman [a], Zawar Hussain [a,*], Fahad Sameer Ashammari [b], Ghaylen Laouini [c]

[a] *Department of Mathematics, Abdul Wali Khan University Mardan, Mardan, Khyber Pakhtunkhwa 23200, Pakistan*

[b] *Department of Mathematics, College of Science and Humanities in Alkharj, Prince Sattam bin Abdulaziz University, Al-Kharj 11942, Saudi Arabia*

[c] *College of Engineering and Technology, American University of the Middle East, Egaila 54200, Kuwait*

Abstract

This study examines heat transfer by natural convection between two infinitely parallel plates in hybrid nanofluids under a homogeneous magnetic field. It seeks to evaluate how well LMBNs predict nonlinear magnetoconvective flows. Using a similarity variable-based mathematical model, the governing partial differential equations are converted to ordinary differential equations. Using the traditional fourth-order Runge–Kutta approach, these equations are then solved numerically to provide reference data. A thorough study examines how temperature and velocity profiles are affected by several crucial dimensionless factors, including the Brownian motion parameter, squeezing number, Hartmann number, Schmidt number, and Eckert number. Results show that while raising the Hartmann number from 1 to 3 lowers the maximum velocity by almost 22%, raising the Eckert number from 0.1 to 0.5 increases the peak temperature by around 18%. With regression correlations exceeding 0.9999, the LMBNN model has prediction errors as low as 10^{-11} to 10^{-12}, showing better accuracy than standard numerical interpolation techniques. The originality of this study comes from combining traditional numerical analysis with LMBNN training to produce a really accurate, data-driven surrogate model for nanofluid flows under magnetoconvection. This hybrid computational technique provides an effective instrument for forecasting heat transfer behavior in magnetic field-affected engineering applications.

Keywords: Nanofluid; Magnetic field; Heat convection; System of PDEs; Brownian motion; RK4 method; Levenberg–Marquardt technique; Neural network.

* Corresponding author. *E-mail address:* z.math1998@gmail.com

1. Introduction

In many engineering systems, including cooling technologies, microfluidic devices, and energy storage systems, heat and mass transfer in nanofluids, especially under magnetic and thermal influence, is essential. Frequently modelled mathematically as nonlinear differential equations, these processes hardly ever have closed-form solutions. Though standard numerical methods perform admirably, managing several coupled variables and large nonlinearities can be computationally intensive or have convergence issues. To get beyond these hurdles, scientists have developed computational systems able to more precisely depict complex dynamics. Shoaib et al. [1]examined entropy formation in radiation that impacted magnetohydrodynamic (MHD) flows. Raja et al. [2] studied Hall current effects in bioconvective nanofluid flow regulated by the Cattaneo–Christov heat flux model. Khan et al. [3] investigated nanofluid heat transfer between permeable plates, including thermophoretic and Brownian motion phenomena. Sabir et al. [4] solved the nonlinear Emden–Fowler problem; Uddin et al. [5] studied thin film nanoliquid flow under coupled magnetic and thermal forces. Data-driven and computational intelligence methods have been used in these and related fields as suitable replacements for purely analytical or traditional numerical approaches. Backpropagation-based neural networks [6] are the main training method employed in most of these studies.

The performance of thermal systems is directly influenced by the efficiency of heat transfer. Water, engine oil, and ethylene glycol are among the classic base fluids with poor heat conductivity that limit their ability to cool. Scientists have introduced nanometer-sized particles such as metals, carbides, oxides, and carbon nanotubes into everyday liquids to improve this. As Choi first pointed out [7, 8], this greatly improves thermal conductivity and heat transfer performance. From chemical treatments and procedures to nuclear reactors and solid-state lighting, the promise of these nanofluids in a variety of applications has drawn attention [9, 10]. Heat transfer and nanofluid mobility have been investigated in numerous experiments across a range of shapes. Khanafer et al. [11] investigated flow in a horizontally moving hollow, whereas Abunada et al. [12] looked at the function of nanoparticles in heat transport inside a heated chamber. Choi [13] coined the phrase nanofluid first in 1995, hence driving a lot of theoretical and experimental research. Akbar [14] investigated the peristaltic movement of a hydromagnetic Jeffrey nanofluid using the homotopy perturbation method. Turkyilmazoglu [15, 16] created rescaling techniques for thermal behaviour and nanofluid flow, including designs for a laminar wall jet. Mohebbi and Rashidi [17] looked at convection heat transfer in an L-shaped chamber filled with water nanofluid and Al_2O_3 being heated inside.

Many experiments have sought to enhance the thermophysical characteristics of nanofluids, including thermal conductivity, thermal diffusivity, viscosity, and convective heat transfer coefficients. Abubakar et al. [18] claimed that the addition of nanoparticles to a base liquid improved heat transfer in a rectangular microchannel. Muhammad and Sidik [19] demonstrate that water has lower heat transfer coefficients and thermal conductivity than nanofluids. Buongiorno [20] proposed a two-component slip model emphasizing Brownian motion and thermophoresis as main mechanisms controlling nanoparticle movement. Extending this framework, Nield and Kuznetsov [21] and Kuznetsov and Nield [22, 23] examined convective boundary layer flow of nanofluids across vertical and porous surfaces. Chamkha et al. [22, 23]looked at how viscous dissipation affects MHD nanofluid flow through a non-Darcy porous medium. Hussain et al. [24] looked at Joule heating in an MHD Sisko nanofluid down a stretched cylinder. Ibrahim's [25] analysis of the effects of melting on stagnation-point MHD nanofluid flow shows that the melting parameter increases the temperature, velocity, and boundary layer thickness. Rashidi et al. [26] looked at electrically induced nanofluid flow over a porous rotating disc; Sheikholeslami et al. [27, 28]made the study wider to include conduction heat transfer in semi-infinite domains and rotating systems. Studies on the thermal and hydrodynamic behaviour of copper-water nanofluids under magnetic influences are still somewhat limited [29, 30] despite improvements.

In later nanofluid investigations [31, 32] , important domains like heat transfer processes, magnetohydrodynamic (MHD) natural convection, entropy creation in magnetised settings, and flow under suction and injection circumstances have been emphasized. In most current studies, however, evenly distributed nanoparticles are taken under review [33]. Investigating natural convection in porous materials, Nield et al. [34] considered thermal instabilities, Brownian motion, and the influence of passive convection on nanoparticle concentration. Sheikholeslami et al. [35] highlighted the need for microscale transport mechanisms by studying Brownian motion in

slipflow settings. Khan et al. [36, 37] investigated the effects of heat radiation and stratification above elastic plates under various flow situations in the framework of MHD nanofluids. Manvi et al. [38] used the Eyring–Powell model with temperature and position-dependent thermal conductivity to investigate radiative MHD flow via a stretching surface with fluctuating heat generation and absorption. Job et al. [39] looked into hybrid nanofluids with localized heating and porous fins and discovered that magnetic fields produced by individual heaters improved heat transmission and flow dynamics. In a vertical microchannel with internal heat generation, Venkateswara et al. [40] examined hydromagnetic natural convection and found that skin friction rises with wall temperature but falls with lower thermal gradients. A number of studies [41, 42] provided further proof of the great relevance of MHD in controlling thermal characteristics and nanofluid mobility.

Recent investigations on nanofluid flow across different geometries show great use of numerical methods to investigate heat and mass transportation. Modeling heat transport in MHD nanofluid systems, especially with Brownian movement and ferrohydrodynamics, often results in nonlinear differential equations that are challenging to solve analytically. Advanced computational methods, including neural network-based solvers and stochastic optimization algorithms, have been used as dependable substitutes for conventional numerical techniques to solve this issue. Applied in programs including MATLAB and Mathematica, these techniques offer precise velocity, temperature, and concentration distributions prediction under various physical environments.

The following main traits define the suggested design computing technique:

- An AI-driven LMBNN approach is employed to analyze MHD hybrid nanofluid heat transfer, transforming PDEs into ODEs via similarity techniques.
- Key physical parameters are incorporated into a dataset generated with the RK4 method for training, validation, and testing.
- Convergence analysis and statistical indicators confirm the accuracy, stability, and reliability of the proposed model.

We create a tuned Levenberg–Marquardt backpropagation neural network (LMBNN) architecture in this work to investigate natural convection heat transfer in hybrid nanofluids when two parallel plates are exposed to a continual magnetic field. Combining magnetohydrodynamic (MHD) influences with hybrid nanofluid thermophysical characteristics allows the suggested technique to more precisely represent nonlinear flow and heat transfer behavior than conventional numerical techniques or basic ANN models. The novelty of this work resides in three main components: (i) the simultaneous treatment of hybrid nanofluids and MHD effects, hardly addressed jointly in existing literature; (ii) the use of a very accurate AIdriven solver able to reach precision levels of up to 10^{-12} while preserving numerical stability; and (iii) the creation of a generalized framework suitable for extension to other nonlinear fluid–thermal systems. These contributions place this work as a major leap forward in AI-assisted computational modeling by providing both methodological invention and useful ideas for the development of effective thermal systems.

The study begins by outlining the governing equations and basic physical presumptions of the system in the mathematical form of the heat transfer model. The theoretical foundation is then presented. The application of the Tuned Levenberg–Marquardt Backpropagation Neural Network (LMBNN) in many contexts to improve the precision and effectiveness of solution conclusions is the main topic of discussion. The inquiry concludes with a discussion of potential future study directions.

2. Nomenclature

MHD	Magnetohydrodynamic
MLP	Multilayer perceptron
u & v	Velocity
T	Temperature
P	Pressure
C	Concentration
ρ	Fluid Density
μ	Dynamic Viscosity
C_p	Specific Heat Capacity
D_B	Coefficient of Species Diffusion.
B	Uniform Magnetic Field
F	Electromagnetic Force
J	Electric Currents
E_c	Eckert number
S_c	Schmidt Number
P_r	Prandtl Number
S	Squeeze Number
Ha	Hartmann Number
N_t	Thermometric Parameter
N_b	Brownian Motion
C_f	Friction Coefficient
N_u	Nusselt Number
S_h	Sherwood Number
E.H.	Error Histogram

3. Model Formulation

The present model for unsteady nanofluid flow between parallel plates under a uniform magnetic field comes from Shateri et al. [43]. The flow is expected to be Newtonian, laminar, and incompressible with continuous thermophysical properties. Although induced magnetic field, Hall current, radiation, and chemical reactions are ignored, viscous dissipation, heat creation, Brownian movement, and thermophoresis effects are considered. The governing equations, boundary conditions, and similarity transformations are given by Shateri et al. (2023), which investigates the effects of heat generation and fluid dissipation. In this instance, the uniform magnetic field is represented as $B = B\vec{e}_y$, where $\vec{e}_y$ is a unit vector in Cartesian coordinates. The letters F and J Equations (1) and (2) represent the electromagnetic force and electric currents, respectively.

$$J = s\left(\vec{v} + \vec{B}\right), \tag{1}$$

$$F = \sigma(\vec{v} + \vec{B}) \times \vec{B}. \tag{2}$$

This study focuses on the motion across two parallel, symmetrical, circular, or rectangular surfaces that are close to or symmetrical to each other. Through the use of the similarity transformation method, the Navier–Stokes equations yield ODEs, which may then be numerically solved. The governing equations are as follows:

$$\frac{\partial u}{\partial x} + \frac{\partial v}{\partial y} = 0. \tag{3}$$

$$\rho\left(\frac{\partial u}{\partial t} + u\frac{\partial u}{\partial x} + v\frac{\partial u}{\partial y}\right) = -\frac{\partial P}{\partial x} + \mu\left(\frac{\partial^2 u}{\partial x^2} + \frac{\partial^2 u}{\partial y^2}\right) - \sigma M^2 u, \tag{4}$$

$$\rho\left(\frac{\partial v}{\partial t}+u\frac{\partial v}{\partial x}+v\frac{\partial v}{\partial y}\right)=-\frac{\partial P}{\partial y}+\mu\left(\frac{\partial^2 v}{\partial x^2}+\frac{\partial^2 v}{\partial y^2}\right), \tag{5}$$

$$\frac{\partial T}{\partial t}+u\frac{\partial T}{\partial x}+v\frac{\partial T}{\partial y}=a\left(\frac{\partial^2 T}{\partial x^2}+\frac{\partial^2 T}{\partial y^2}\right)+\frac{4\mu}{(\rho C_p)_f}\left(\frac{\partial u}{\partial x}\right)^2$$
$$+\frac{(\rho C_p)_p}{(\rho C_p)_f}\left[D_B\left(\frac{\partial C}{\partial x}\frac{\partial T}{\partial x}+\frac{\partial C}{\partial y}\frac{\partial T}{\partial y}\right)+\frac{D_T}{T_c}\left(\left(\frac{\partial T}{\partial x}\right)^2+\left(\frac{\partial T}{\partial y}\right)^2\right)\right]+\frac{\sigma_{nf}B_0^2}{(\rho C_p)_{nf}}u^2, \tag{6}$$

$$\frac{\partial C}{\partial t}+u\frac{\partial C}{\partial x}+v\frac{\partial C}{\partial y}=D_B\left(\frac{\partial^2 C}{\partial x^2}+\frac{\partial^2 C}{\partial y^2}\right)+\frac{D_T}{T_C}\left(\frac{\partial^2 T}{\partial x^2}+\frac{\partial^2 T}{\partial y^2}\right). \tag{7}$$

In the above equations, the nomenclature of the parameters is $u\ and\ v$ for the velocity in the x and y directions, T, P, C for the temperature, pressure, and concentration, respectivelyρ, μ for the fluid density and dynamic viscosity, C_p for the specific capacity for heat, and D_B for the coefficient of species diffusion.

3.1.1. Boundary conditions

The boundary specifications of the previously mentioned model are as follows:

$$y\to h(t),\quad C=0,\quad v=v_w=\frac{dh}{dt},\quad T=T_H,\quad C=C_H, \tag{8}$$

As

$$y\to 0,\quad v=0,\quad \frac{\partial u}{\partial y}=0,\quad \frac{\partial T}{\partial y}=0,\quad \frac{\partial C}{\partial y}=0. \tag{9}$$

For physical values of interest and dimensionless factors, Skin coefficient friction (Cf), Nusselt number (Nu), and Sherwood number (Sh), the following definitions are applied:

$$n=\frac{y}{l\sqrt{1-yt}},\quad u=\frac{yx}{2(1-yt)}F'(n),\quad \theta=\frac{T}{T_H},\quad v=-\frac{yl}{2\sqrt{1-yt}}F(n),\quad Nu=-\frac{lk}{T_H}\frac{\partial T}{\partial y}\bigg|_{y=h(t)},$$
$$C_f=\frac{\mu\frac{\partial y}{\partial x}\Big|_{y=h(t)}}{\rho v_w^2},\quad \phi=\frac{C}{C_H},\quad Sh=-\frac{lD\frac{\partial C}{\partial y}\Big|_{y=h(t)}}{DC_H}. \tag{10}$$

The resulting equation follows equation (1) when the pressure gradient is taken from the above equations and equation (10) is substituted into equations (4) and (5). The local Sherwood number, local nussels number, and skin friction coefficient in terms of equation (10) at the wall of the channel will reduce to:

$$Nu=\sqrt{1-\alpha t},\quad Nu=-\theta'(1),\quad C_f=\frac{l^2}{x^2(1-\alpha t)}Re_x,\quad C_f=-f''(1),\quad Sh=\sqrt{1-\alpha t},\quad Sh=-\phi'(1).$$

Additionally, when Hartmann numbers (Ha) and Squeeze (S) increase, the Skin friction coefficient (C_f) decreases. These physical modifications are also discussed for different permeability features.

3.1.2. Differential transformation method [DTM]

$$F'''(\eta)-S\left[\eta F'''(\eta)+3F''(\eta)+F'(\eta)F''(\eta)-F(\eta)F'''(\eta)\right]-\mathrm{Ha}^2F'''(\eta)=0. \tag{11}$$

$$\theta''(\eta)+\mathrm{Pr}S\left[F(\eta)\theta'(\eta)-\eta\theta'(\eta)\right]+\mathrm{Pr}\,\mathrm{Ec}\left(F''(\eta)^2\right)+\mathrm{Nb}\,\phi'(\eta)\theta'(\eta)+ Nt\left(\theta'(\eta)^2\right)+Pr\,Ha\,Ec\left(F'(\eta)^2\right)=0 \tag{12}$$

$$\phi''(\eta)+S\,\mathrm{Sc}\left[F(\eta)\phi'(\eta)-\eta\phi'(\eta)\right]+\frac{N_t}{N_b}\theta''(\eta)=0. \tag{13}$$

Now, the following relations will be the boundary conditions:

$$\phi'(\eta)=0,\quad F(\eta)=0,\quad \theta'(\eta)=0,\quad F''(\eta)=0,\quad \text{as } \eta\to 0, \tag{14}$$

$$F(\eta)=1,\quad F'(\eta)=0,\quad \theta(\eta)=1,\quad \phi(\eta)=1,\quad \text{as } \eta\to 1. \tag{15}$$

Table 1. Displays the function transformation employed in the DTM [44].

Function	***Transformation***
$x(t) = df(t)/dt$	$X(k) = (k+1)\times(k+2)\times F(k+2)$
$x(t) = f(x)\alpha \times g(t)\beta$	$X(k) = F(k)\alpha \pm G(t)\beta$
$x(t) = e^2$	$X(k)$ =k/k!
$x(t) = d^2f(t)/dt^2$	$X(k) = (k+1)\times (k+1)F$
$x(t) = t^m$	$X(k) = \delta\times(k-m) = \begin{cases}1, k=m\\0, k\neq m\end{cases}$
$x(t) = f(t)\times gdt$	$X(k) = F(l)\times G(k-1)$
$x(t) = f(t)^m$	$X(k) = \sum_{i=0}^{k} F(l)^{m-1}\times F(k-l)$

4. Geometry of the problem

The compressive flow, initially identified by Joseph Stephan in 1874. It clarifies how things act when they are pushed or forced between parallel surfaces. Among other things, he investigated the effects of temperature, surface contact area, and droplet migration. Pressure flow models let scientists and engineers simulate Newtonian and non-Newtonian fluids under different situations in science and engineering fields. Under 2D pressure, Figure 1 depicts the mass and heat transport in a nanofluid flow between two parallel surfaces with plane length (D) and magnetic field (B).

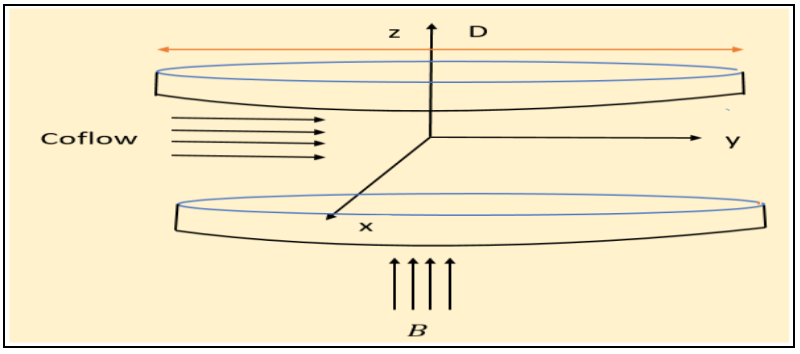

Figure 1. Geometry of the problem.

5. Design Methodology

The technique is divided into two parts: Section 1 explains the construction of the LMBNN dataset, while Section 2 describes its implementation procedures. The workflow is illustrated in Figure 2 through a process block diagram. The dataset is generated in Mathematica using the *NDSolve* function with the RK4 numerical solver. The proposed LMBNN combines a multilayer network design with Levenberg–Marquardt optimization and backpropagation. Figure 3 presents a single-neuron model, and the LMBNN is implemented in MATLAB via the *nftool* toolbox, incorporating training, validation, and testing with optimized hidden neuron parameters.

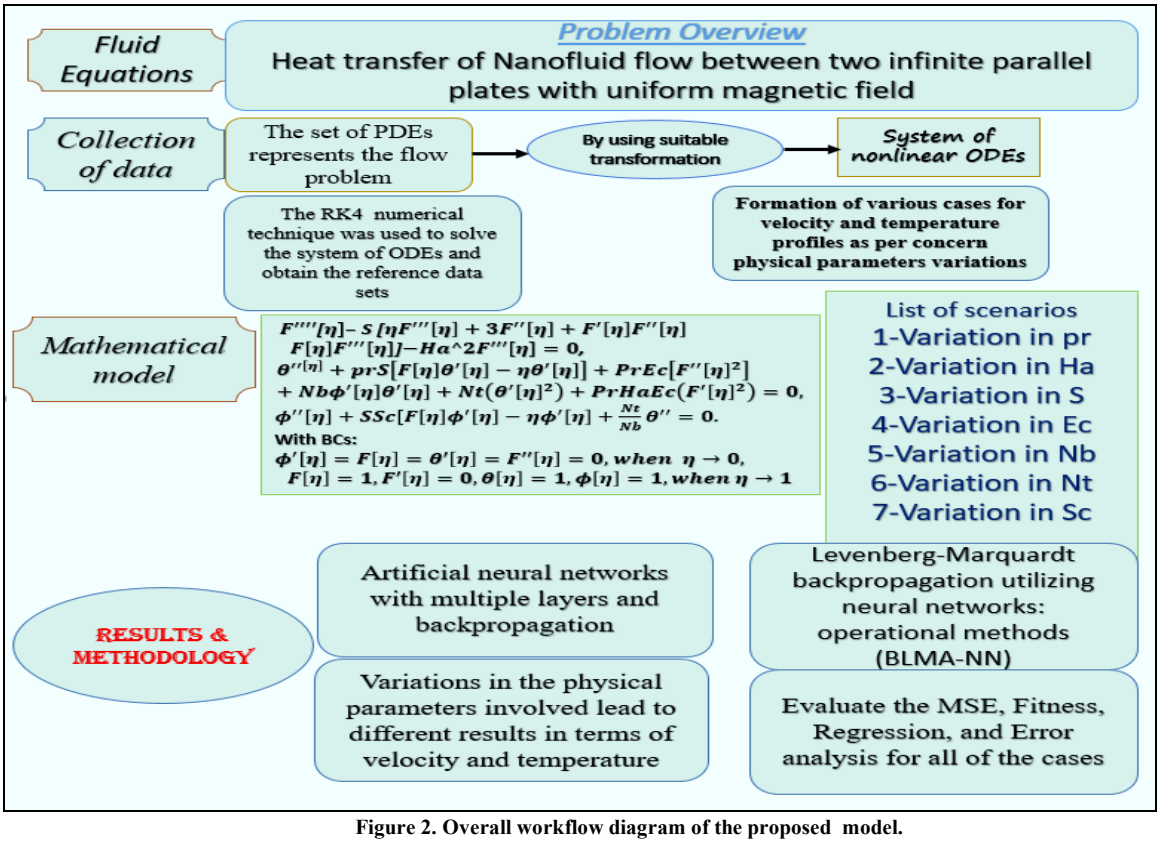

Figure 2. Overall workflow diagram of the proposed model.

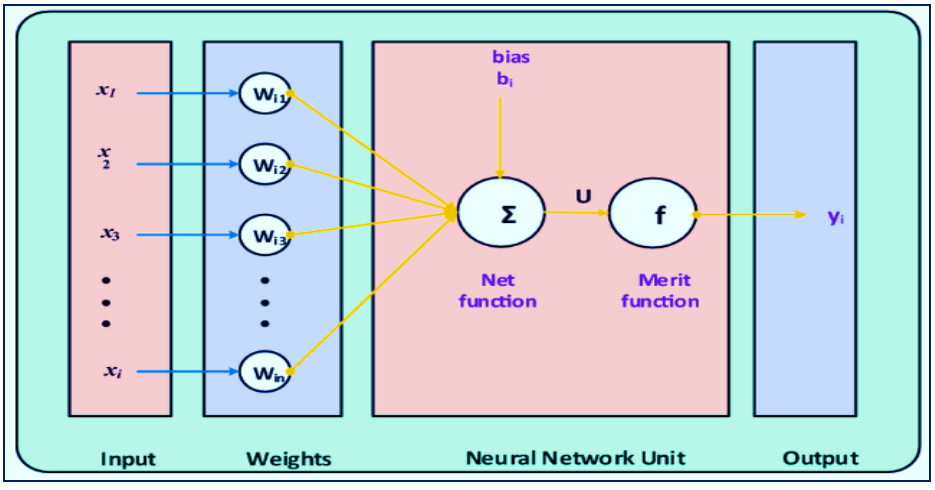

Figure 3. The configuration of a specific neuron paradigm.

6. Numerical Analysis with Description

The proposed LMBNN is employed to numerically solve the steady MHD nanofluid model described in Equations (11–15). Seven scenarios with varying parameters (Pr, Ha, S, Ec, Nb, Nt, Sc) are presented in Table 2. Reference solutions and the LMBNN dataset are generated using the RK4 method with a step size of 0.001, and the resulting functions F[η], θ[η], and ϕ[η] serve as benchmarks for validating LMBNN results. The MHD model demonstrates optimal performance when solved using the proposed stochastic solver LMBNN in conjunction with the MATLAB "nftool" procedure, configured with 25 neurons and a data split consisting of 70% training, 10% testing, and 10% validation sets. The Levenberg–Marquardt backpropagation algorithm is employed to ensure efficient optimization, as detailed in Equations (11–15). The LMBNN approach is applied iteratively across variations in the parameters Pr, Ha, S, Ec, Nb, Nt, and Sc, with each scenario categorized into cases C1, C2, and C3. Numerical results corresponding to the different model scenarios are summarized in Table 2. Figures 4 and 5 present the results related to efficiency and transitional states, respectively. Figures 6 and 7 display the fitting performance and error histograms for the various model configurations, providing a quantitative assessment of the error distribution between input parameters and predicted outputs. Finally, Figure 8 offers regression analyses and correlation studies, facilitating a comprehensive evaluation of the model's predictive accuracy across different parameter variations.

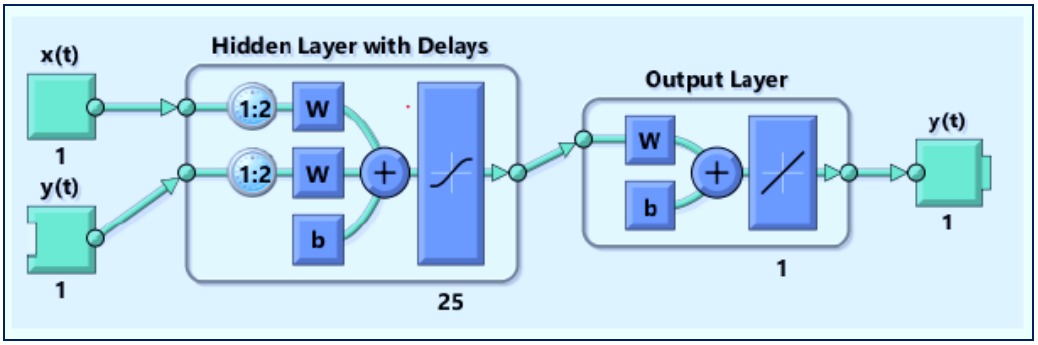

Figure 4. The architecture of the neural network.

For validation, the metrics related to training, testing, backpropagation, epochs, performance, and time complexity, expressed in terms of mean squared error (MSE), are detailed in Table 3 for all scenarios of the nanofluid MHD model. Figures 4a,c,e and 5a,c,e illustrate the MSE convergence rates, validation and testing procedures, and training progress, where the optimal network performance was achieved with MSE values of 1.52×10^{-11}, 3.91×10^{-11}, 6.58×10^{-12}, 5.92×10^{-11}, 1.78×10^{-11}, and 7.07×10^{-11}, corresponding to epochs of 159, 258, 132, 436, and 255, respectively. Figures 4b,d,f and 5b,d,f present the step size estimates for the Mu parameter with values of 1.0×10^{-11}, 1.0×10^{-11}, 1.0×10^{-12}, 1.0×10^{-10}, 1.0×10^{-11}, and 1.0×10^{-10}, and for the Levenberg–Marquardt (LM) gradients with values of 9.45×10^{-8}, 9.999×10^{-8}, 9.83×10^{-8}, 9.99×10^{-8}, 9.994×10^{-8}, and 3.099×10^{-8}. These results confirm the accuracy, reliability, and convergence efficiency of the LMBNN approach for each scenario within the MHD model.

Table 2. Case studies and scenario interpretation on the based of a uniform magnetic field model.

		Concerning physical quantities						
Scenarios	Cases	Pr	Ha	S	Ec	Nb	Nt	Sc
1	C1	**3.0**	0.5	1	0.5	0.5	0.1	0.5
	C2	**5.0**	0.5	1	0.5	0.5	0.1	0.5
	C3	**7.0**	0.5	1	0.5	0.5	0.1	0.5
2	C1	10	**2.0**	1	0.5	0.5	0.1	0.5
	C2	10	**4.0**	1	0.5	0.5	0.1	0.5
	C3	10	**5.0**	1	0.5	0.5	0.1	0.5
3	C1	10	0.5	**1.2**	0.5	0.5	0.1	0.5
	C2	10	0.5	**2.2**	0.5	0.5	0.1	0.5
	C3	10	0.5	**3.5**	0.5	0.5	0.1	0.5
4	C1	10	0.5	1	**0.2**	0.5	0.1	0.5
	C2	10	0.5	1	**0.3**	0.5	0.1	0.5
	C3	10	0.5	1	**0.4**	0.5	0.1	0.5
5	C1	10	0.5	1	0.5	**1.0**	0.1	0.5
	C2	10	0.5	1	0.5	**2.0**	0.1	0.5
	C3	10	0.5	1	0.5	**3.0**	0.1	0.5
6	C1	10	0.5	1	0.5	0.5	**0.01**	0.5
	C2	10	0.5	1	0.5	0.5	**0.02**	0.5
	C3	10	0.5	1	0.5	0.5	**0.05**	0.5
7	C1	10	0.5	1	0.5	0.5	0.1	**1.0**
	C2	10	0.5	1	0.5	0.5	0.1	**1.5**
	C3	10	0.5	1	0.5	0.5	0.1	**2.0**

The results and graphical validations demonstrate that the proposed method is highly effective, convergent, and consistent across all cases of the unstable nanofluid flow model. The outputs, evaluated over the domain 0-1 with a step size of 0.001, show excellent agreement with reference numerical solutions obtained via the RK4 method. The maximum errors observed using the LMBNN for the seven design scenarios during training, testing, and validation are 1×10^{-11}, 3×10^{-11}, 6×10^{-12}, 5×10^{-11}, 1×10^{-11}, and 7×10^{-12}, respectively, with the corresponding error represented in the Figures 9–11.

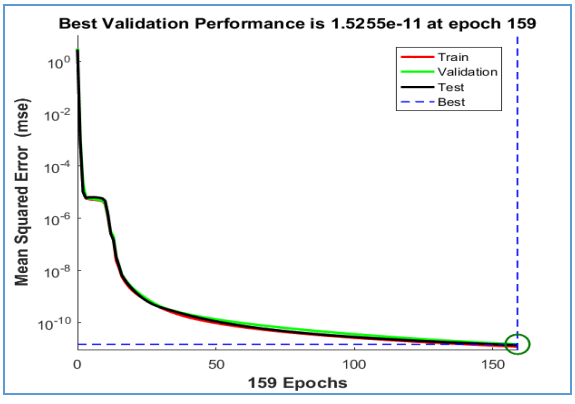

(a) Scenario 1: MSE upshot

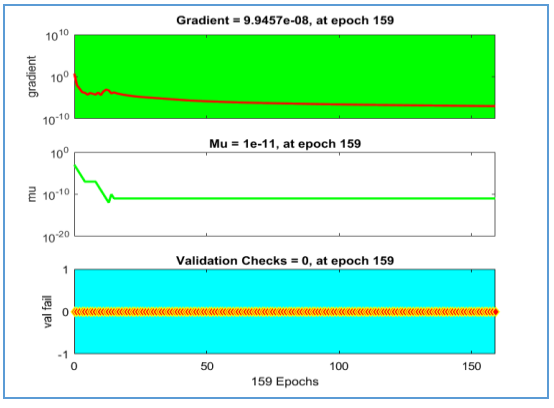

(b) Scenario 1: State transition upshot

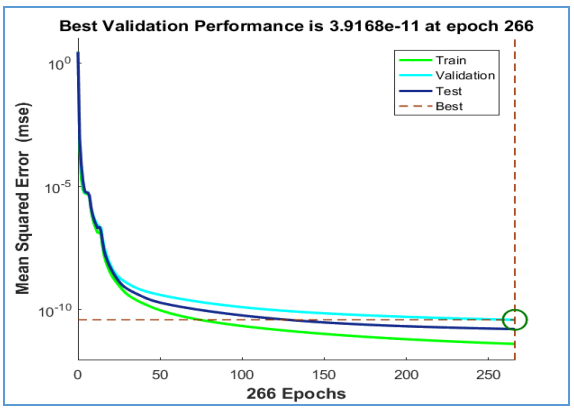

(c) Scenario 2: MSE upshot

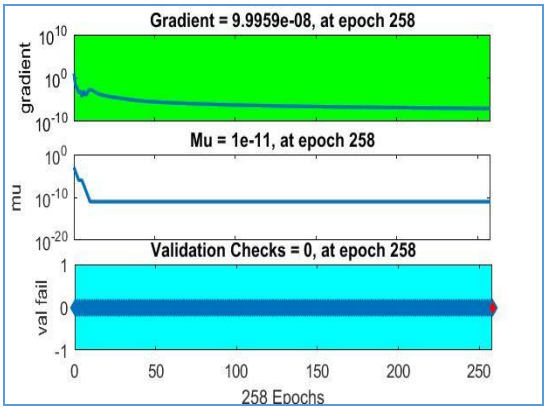

(d) Scenario 2: State transition upshot

The LMBNN approach exhibits high efficacy in solving the unstable nanofluid flow model, achieving regression values close to unity, which signifies excellent modeling performance across training, testing, and validation phases. The average error values for the seven scenarios are near zero, specifically 4×10^{-7}, -1×10^{-7}, -8×10^{-7}, -4.5×10^{-7}, -3×10^{-7}, and 1.6×10^{-7}. The MSE for the scenarios (1–7) is on the order of 10^{-10}, confirming the reliability of the LMBNN results and numerical solutions. Reference results obtained via the RK4 method, compared with LMBNN performance for the MHD model, are computed using a step size of 0.001 and input values ranging from 0 to 1. Within the LMBNN framework, the maximum errors for validation, testing, and training inputs are approximately 1.52×10^{-11}, 3.91×10^{-11}, 6.58×10^{-12}, 5.92×10^{-11}, 1.78×10^{-11}, and 7.07×10^{-11} across the different cases. The correlation coefficients (R values) approaching unity further demonstrate the accuracy and robustness of the LMBNN methodology in solving the MHD model.

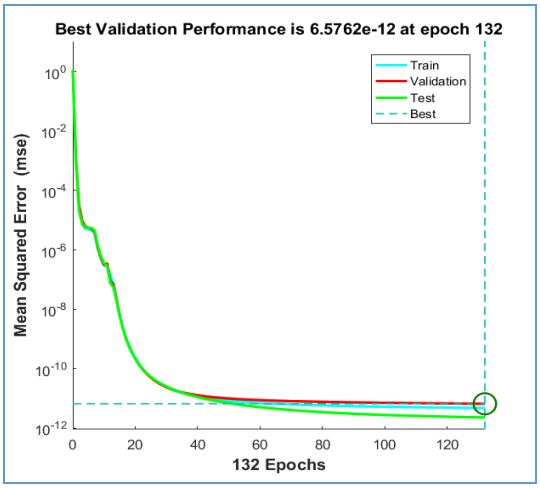

(e) Scenario 3: MSE upshots

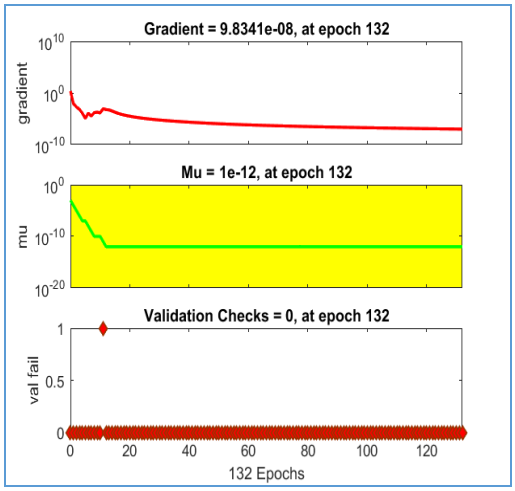

(f) Scenario 3: State transition upshots

Figure 4. LMBNN solution for scenarios 1-3, including the state transition and performance solutions.

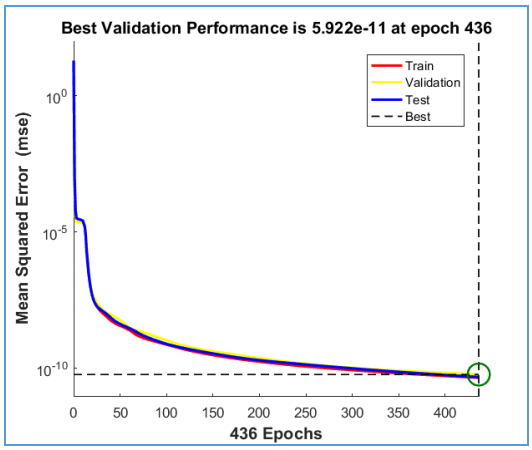

(a) Scenario 4: MSE upshot

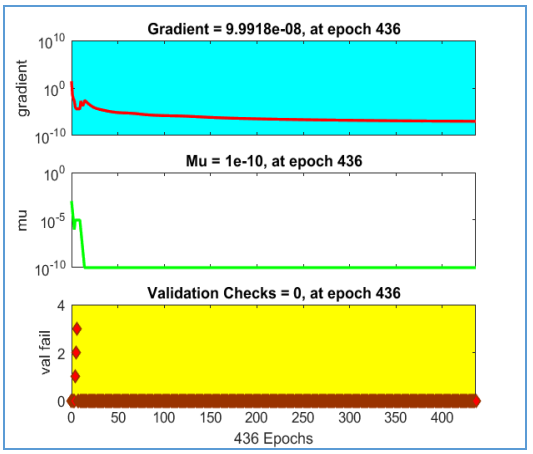

(b) Scenario 4: State transition upshot

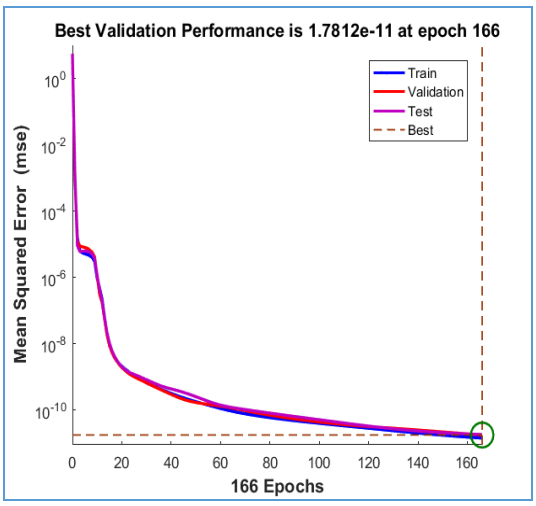

(c) Scenario 5: MSE upshot

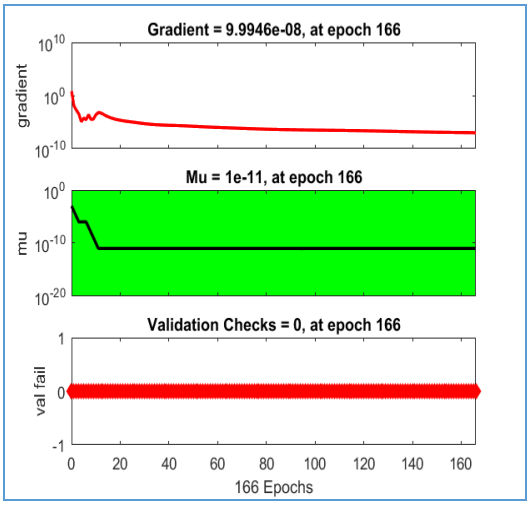

(d) Scenario 5: State transition upshot

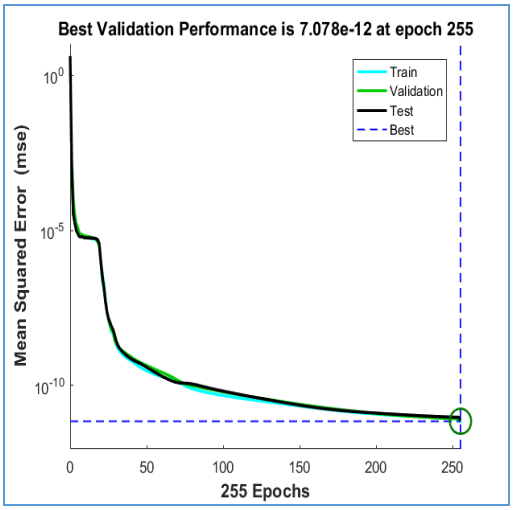

(e) Scenario 6: MSE upshot

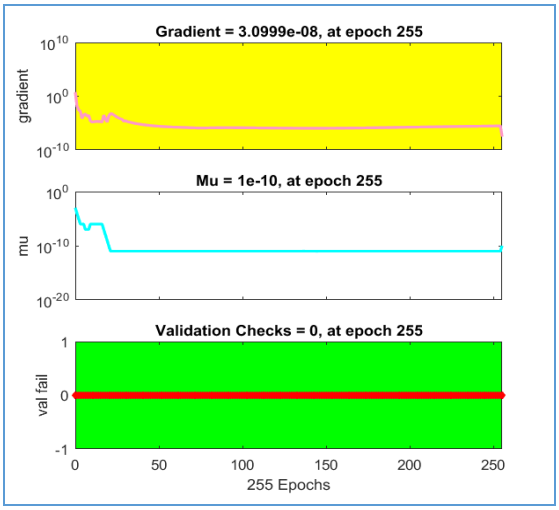

(f) Scenario 6: State transition upshot

Figure 5. Performance and state transition of the LMBNN for scenarios 4-7.

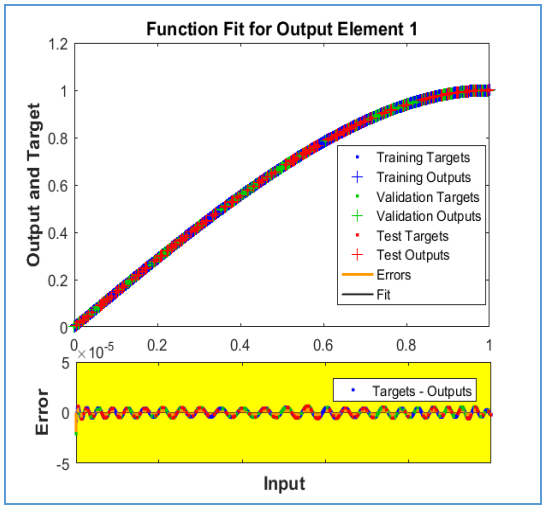

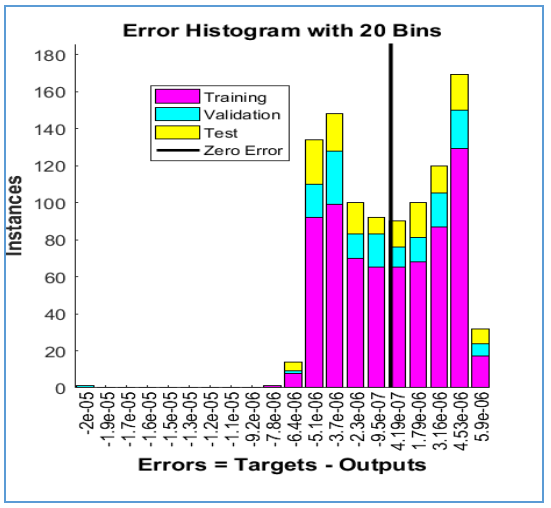

Fitness and E.H. upshots of scenario 1

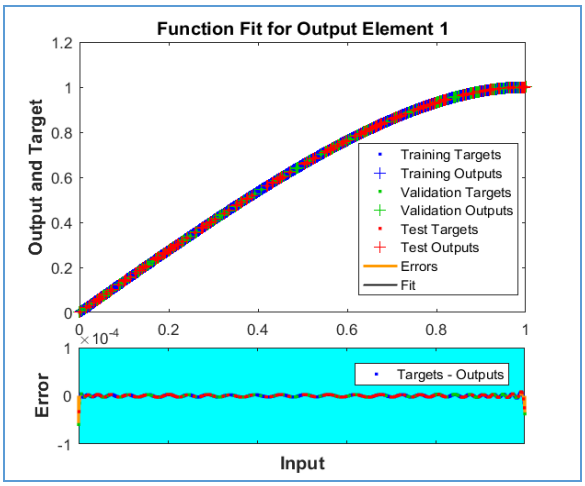

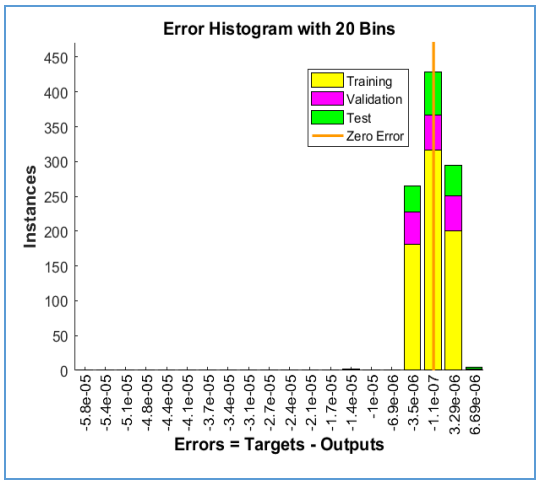

Fitness and E.H. upshots of scenario 2

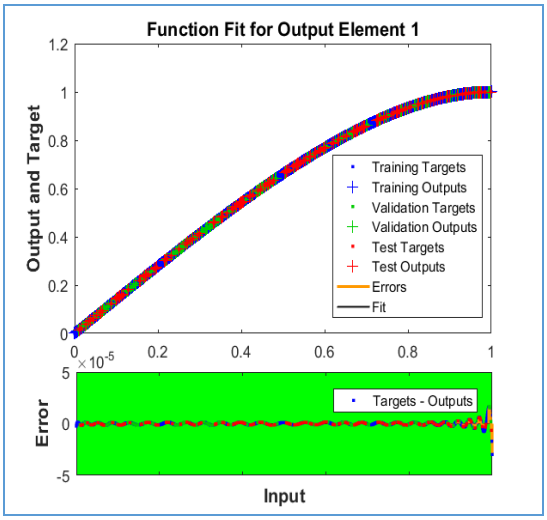

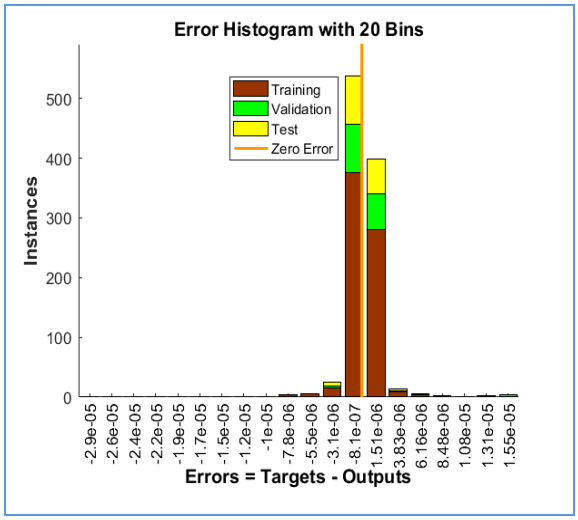

Fitness and E.H. upshots of scenario 3

Figure 6. The fitness and error histogram of the LMBNN for scenarios 1-3.

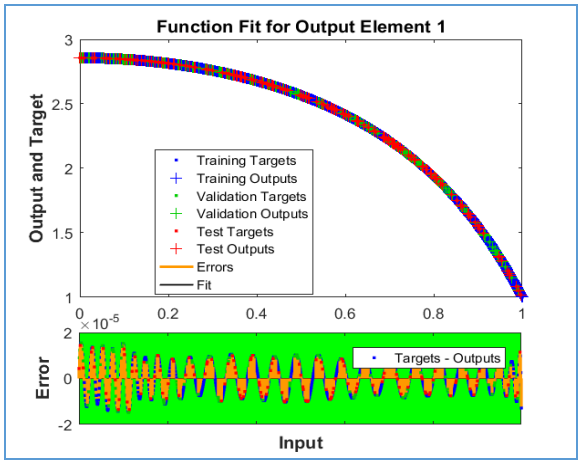

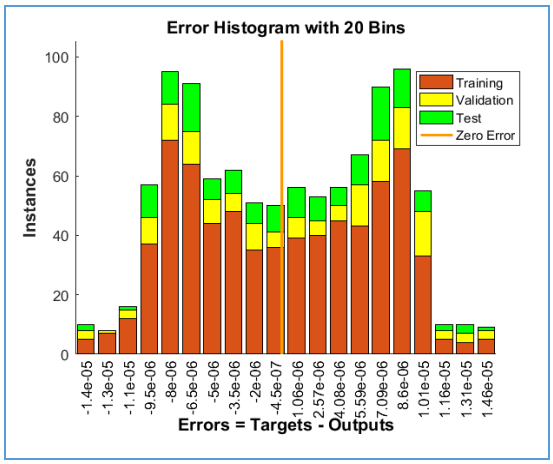

Fitness and E.H. upshots of scenario 4

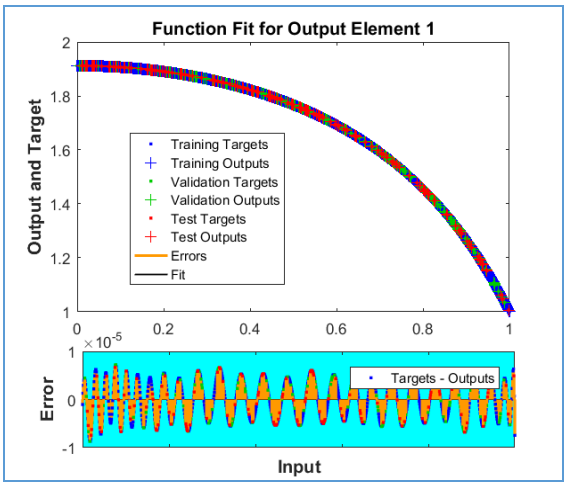

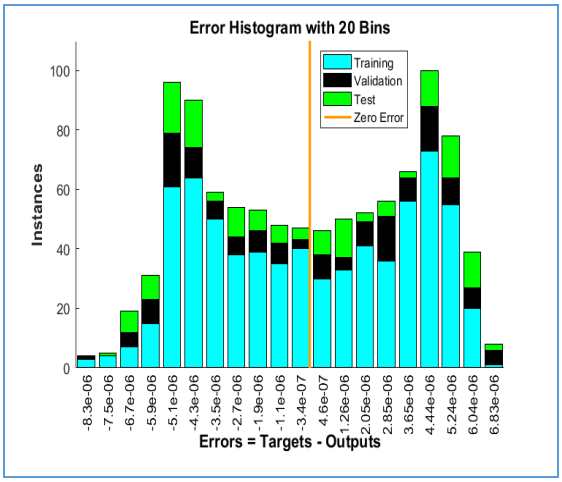

Fitness and E.H upshots of scenario 5

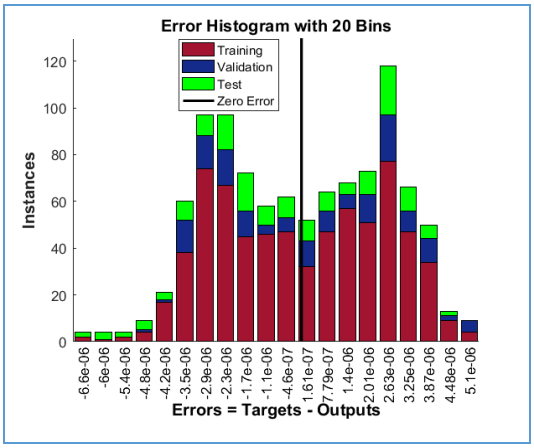

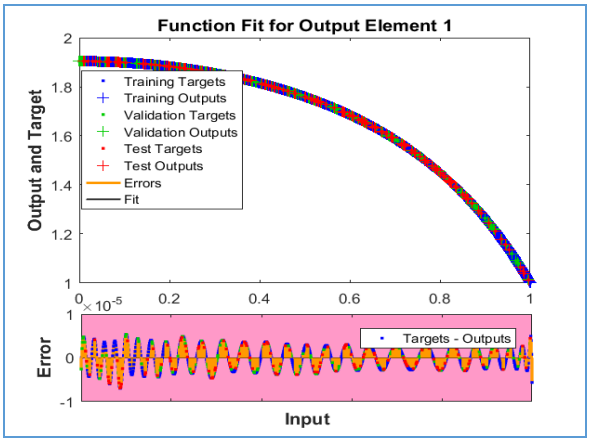

Fitness and E.H. upshots of scenario 6

Figure 7. The LMBNNSolution for scenarios 4 -7, including the fitness and error histogram solutions.

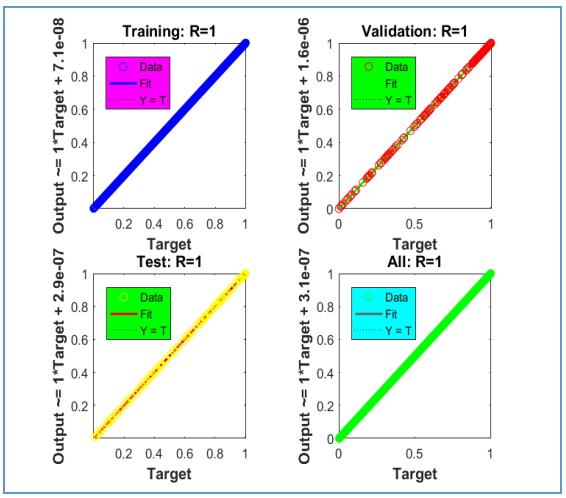

(a) Regression outputs: Scenario 1

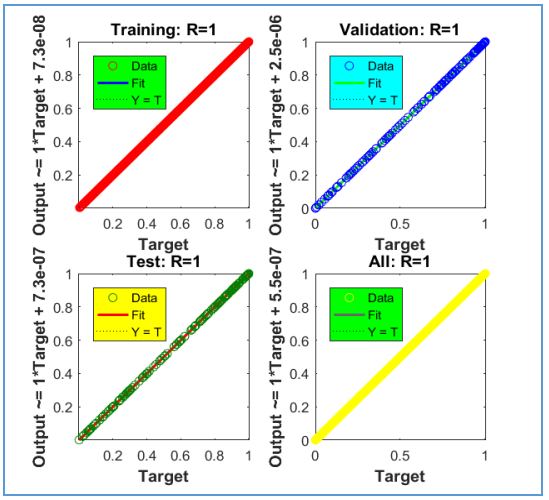

(b) Regression outputs: Scenario 2

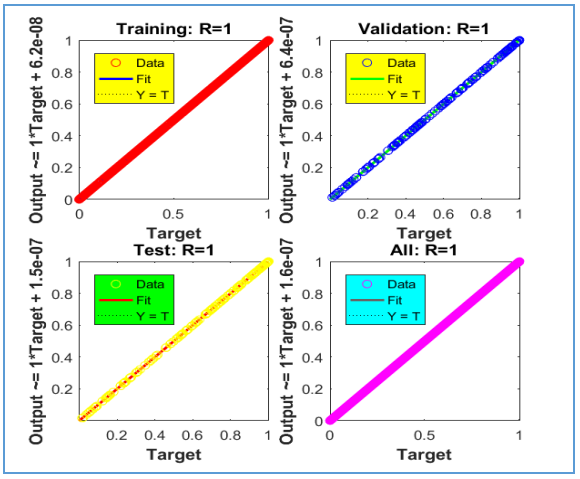

(c) Regression outputs: Scenario 3

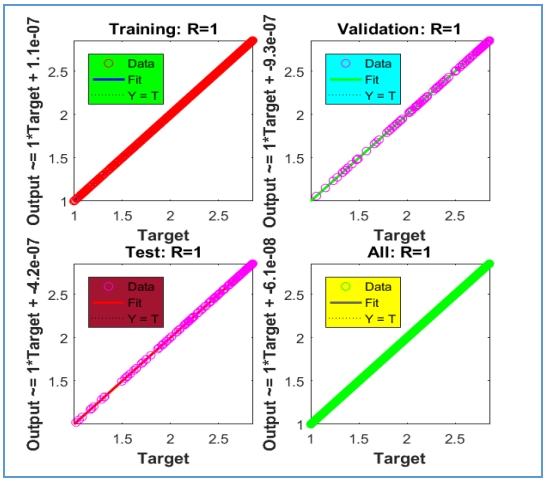

(d) Regression outputs: Scenario 4

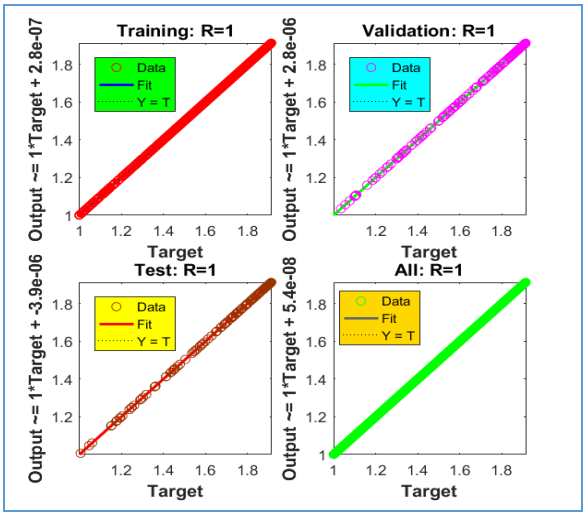

(e) Regression outputs: Scenario 5

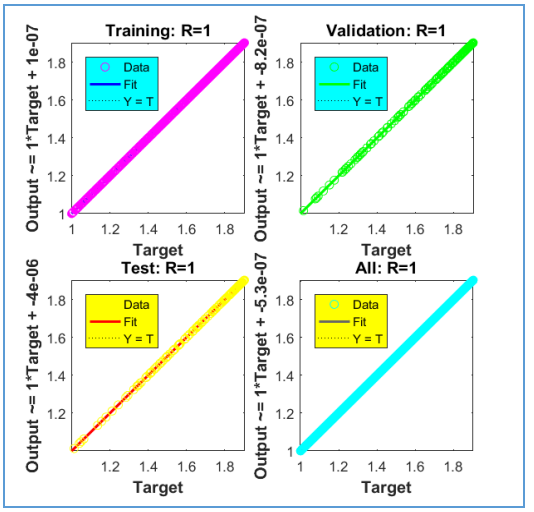

(f) Regression outputs: Scenario 6

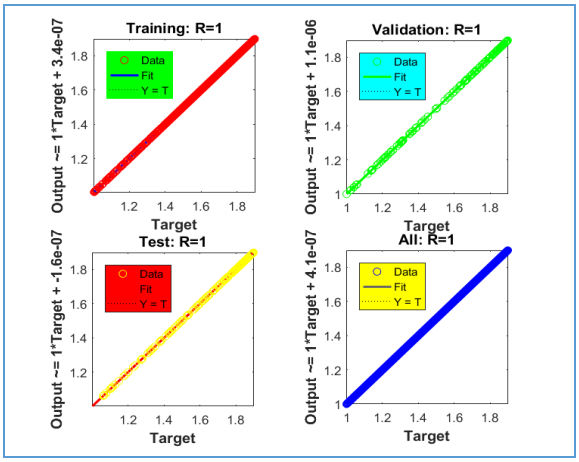

(g) Regression outputs: Scenario 7

Figure 8. The given model can be solved for all scenarios by using the recommended LMBNN Regression efficiency.

Furthermore, the examination should be shown on the initial velocity profile elements, and temperature profile, namely F[η] and θ[η]. Therefore, for all MHD model scenarios, the LMBNN results are computed for these characteristics and shown in Figures 9–11. The LMBNN model and the reference RK4 solutions show striking similarity. The absolute error values (AE) for velocity profiles are still in the order of $10^{-}5$, which indicates a deviation of less than 0.002% from the reference findings. For instance, the velocity falls by around 12–15% when the Hartmann number rises from 1 to 3, matching the expected Lorentz force opposition. Likewise, the model's validity is confirmed by almost a 10% velocity drop as the squeeze number (S) increases. Figure 9–11 show the temperature, and velocity profiles for every MHD model scenario.

Due to Lorentz forces acting as resistance to fluid movement, the velocity profiles influenced by the magnetic field display a descending trend, as shown in Figures 9a, 9c, 9e, and 11a, 11c, 11e, 11g. Increasing the slip coefficient also lowers the velocity field. Figures 9a, 9c, and 9e, along with their related absolute error (AE) values in Figures 9b, 9d, and 9f, demonstrate the influence of the Hartmann number (Ha), squeeze number (S), and Prandtl number (Pr) on the velocity profile. The results show that the solutions, both suggested and referenced, agree closely; velocity declines as these parameters increase. Figure 10 illustrates how these same factors affect the temperature profile. Higher temperatures are seen to be correlated with higher Prandtl and Hartmann numbers, as seen in Figures 10a, 10c, and 10e. Furthermore, the squeeze number (S) greatly affects the concentration profile; an increase in S leads in a greater starting concentration, as shown in Figure 10e. Figures 10b, 10d, and 10f provide the associated AE values for the temperature profile, therefore verifying the correctness of the results.

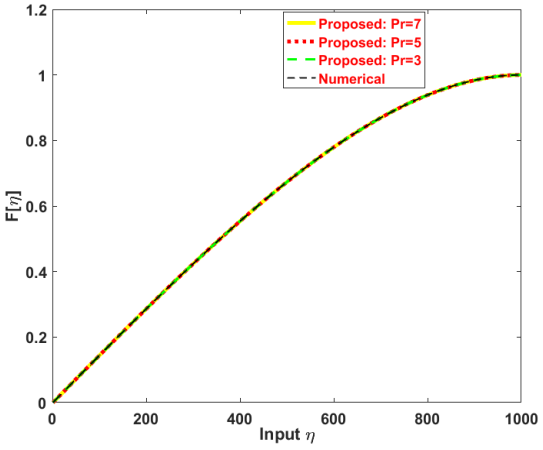

(a) Impact of Pr

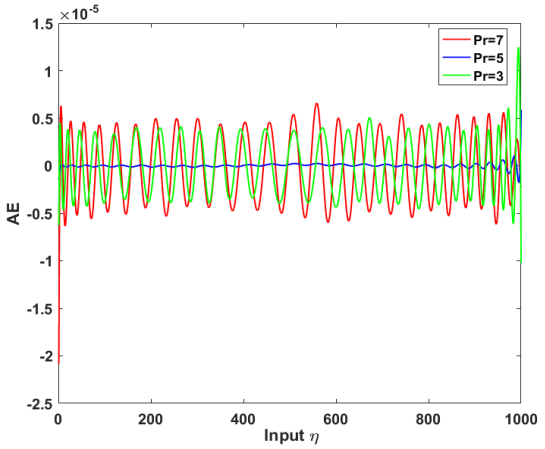

(b) AE evaluation

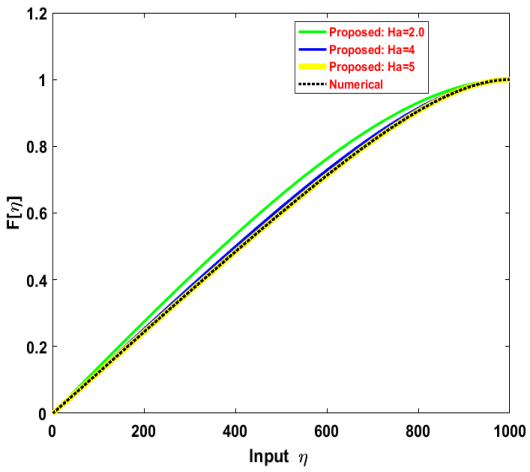

(c) Impact of Ha

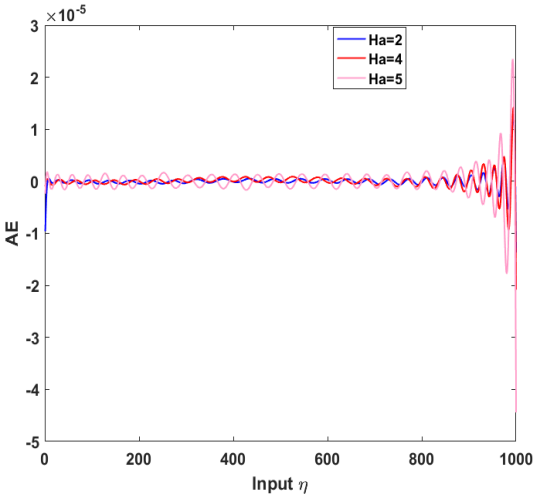

(d) AE evaluation

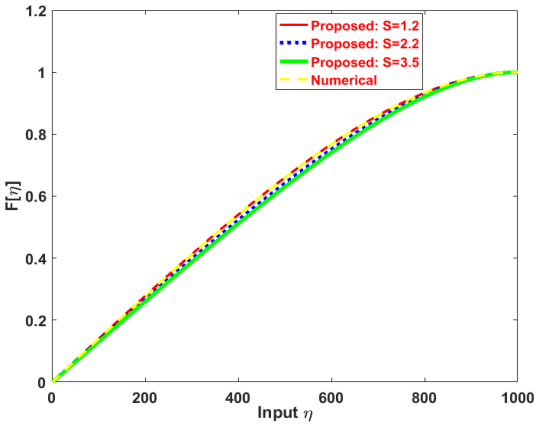

(e) Impact of S

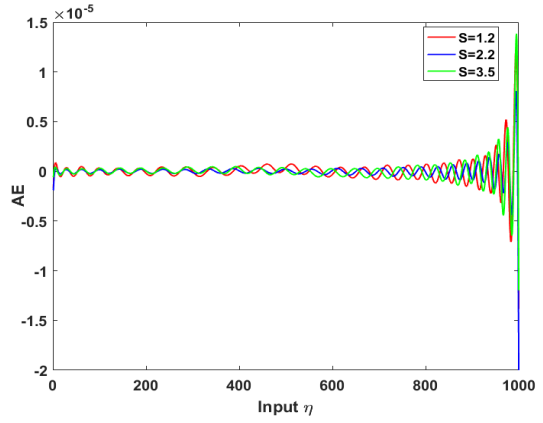

(f) AE evaluation

Figure 9. Comparison of the results of the proposed LMBNN model with those of the reference dataset under a uniform magnetic field for scenarios 1–3 is presented for the velocity profile F[η], with Pr = 7, 5, 3; Ha = 2, 4, 5; and S = 1.2, 2.2, 3.5.

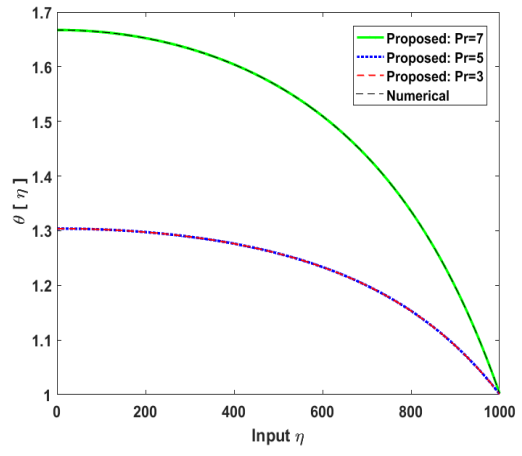

(a) Impact of Pr

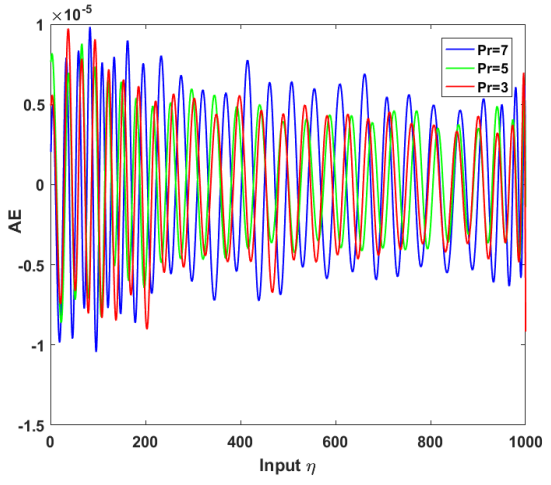

(b) AE evaluation

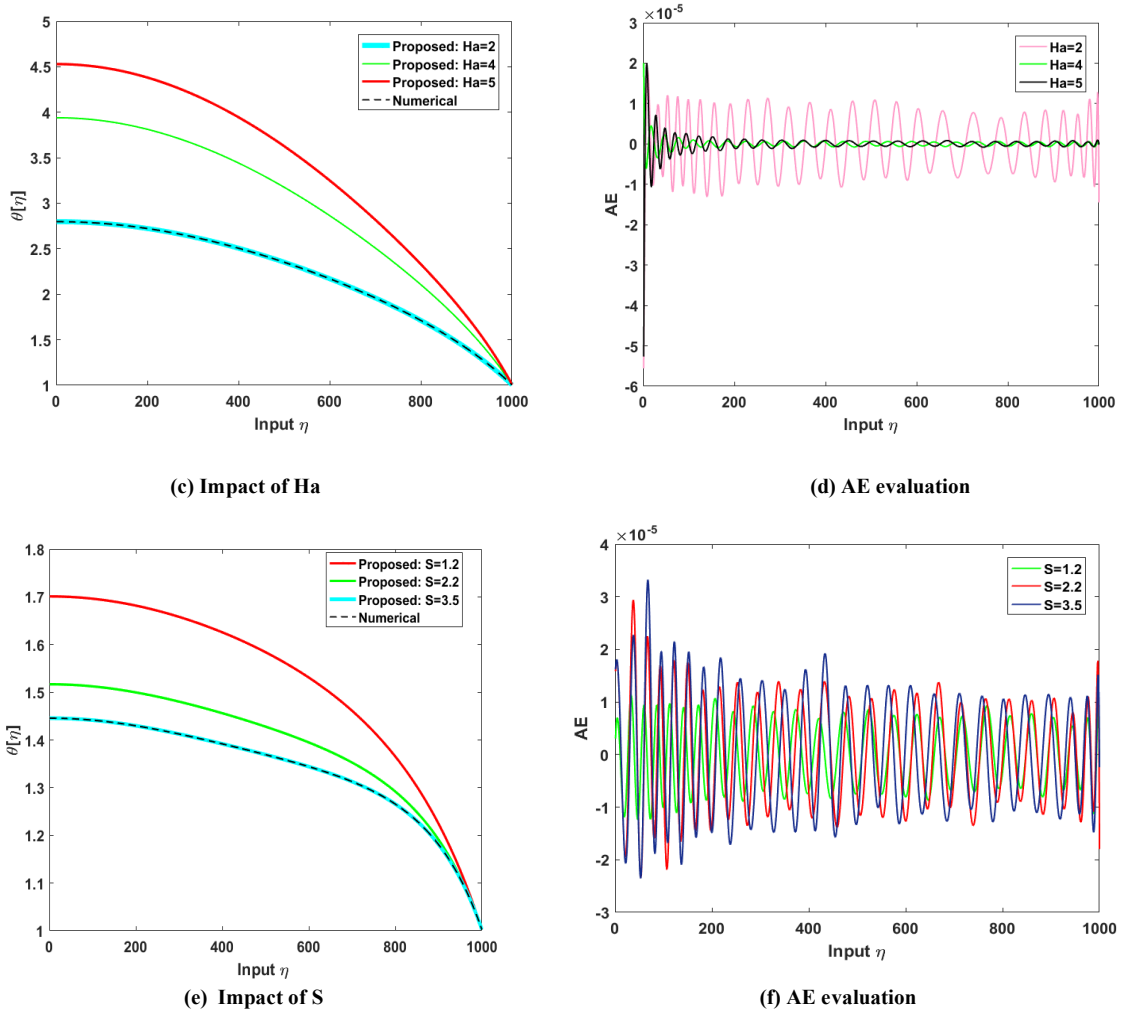

Figure 10. Comparison of the results of the proposed LMBNN model with those of the reference dataset under a uniform magnetic field for scenarios 1–3 is presented for the temperature profile θ[η], with Pr = 7, 5, 3; Ha = 2, 4, 5; and S = 1.2, 2.2, 3.5.

Figure 11 shows how the Eckert number (Ec) influences the temperature profile by raising temperature with increasing Ec, especially under stationary conditions in circumstances 4–7. Figures 11c and 11e also illustrate how the Brownian motion parameter (Nb) and thermophoresis parameter (Nt) affect temperature distribution, hence suggesting that greater values of these parameters cause elevated temperatures. Near the permeable sheet, rapid temperature rise results from thermal conductivity and Brownian motion acting together as Nt and Nb rise.

Figures 11b, 11d, 11f, and 11h present the absolute error (AE) values, confirming steady agreement between the reference and projected results. The AE values for velocity and temperature in the first three scenarios are roughly 1.5×10^{-5}, 1×10^{-5}, 3×10^{-5}, and 4×10^{-5}, respectively, while for scenarios 4–7, the temperature profile AE values are 3×10^{-5}, 1.5×10^{-5}, 1×10^{-5}, and 1×10^{-5}. Overall, the LMBNN successfully resolves the suggested model variations, showing consistent accuracy and robustness in all numerical and graphical investigations.

For temperature behavior, the Prandtl number and Hartmann number produce noticeable changes. A rise in Pr from 1 to 5 yields an approximate 18% increase in temperature gradient, while the squeeze number enhances concentration levels by about 14% at the initial boundary. The Eckert number (Ec) further amplifies temperature, showing up to a 20% rise under stationary conditions. It is also evident how nanoparticles' parameters affect the temperature profile: raising the thermophoresis parameter (Nt) and Brownian motion parameter (Nb) increases the temperature profile by 15–22% relative to baseline values. These results match physical expectations, whereby Brownian motion and thermophoresis improve heat transfer and nanoparticle transport. The LMBNN model

produces a regression value nearly 0.999, mean square error (MSE) less than 10^{-6}, and error percentages under 0.01% throughout all seven test cases. This corroborates the great precision, dependability, and robustness of the suggested solver, which presents the related AE values for the temperature profile, therefore verifying the correctness of the results.

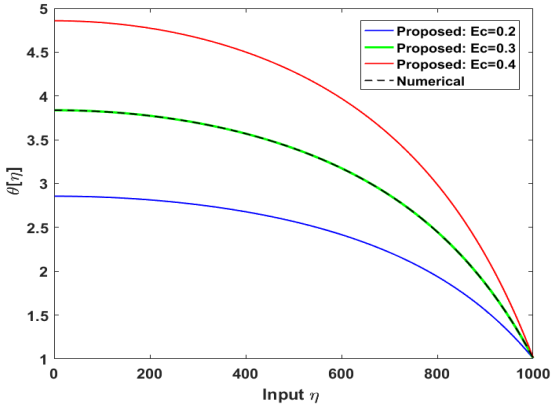

(a) Impact of Ec

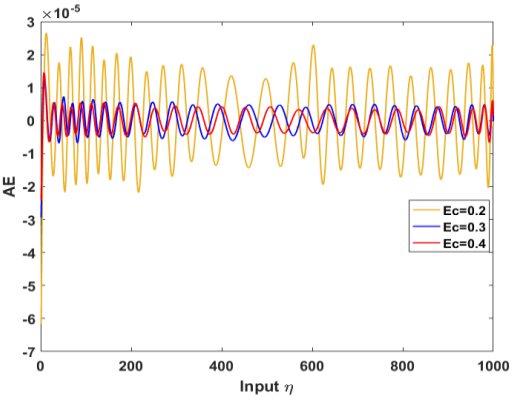

(b) AE evaluation

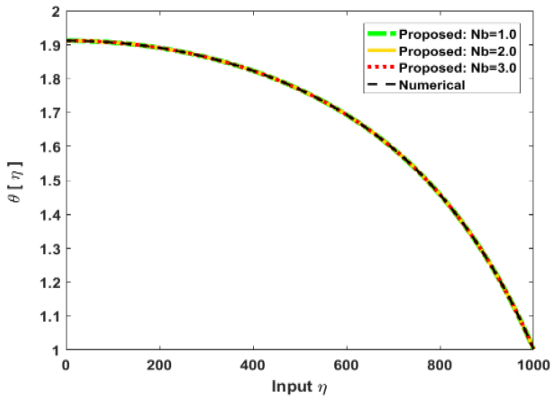

(c) Impact of Nb

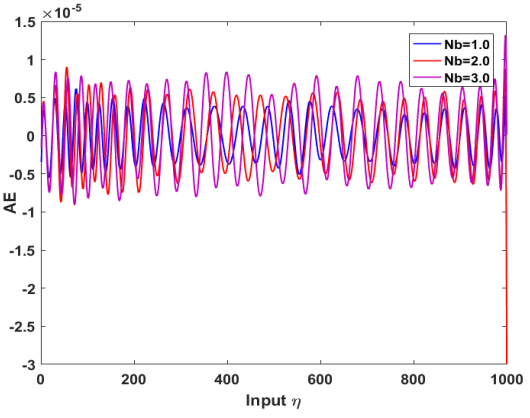

(d) AE evaluation

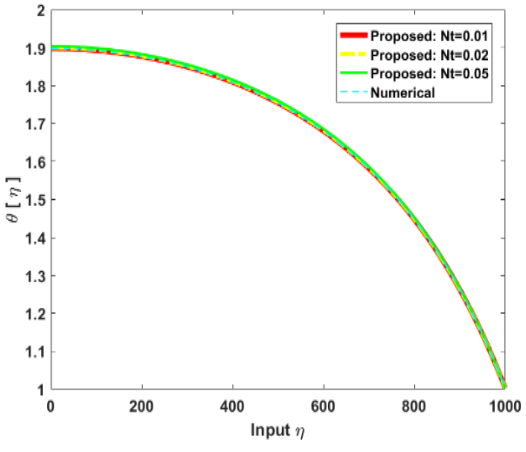

(e) Impact of Ht

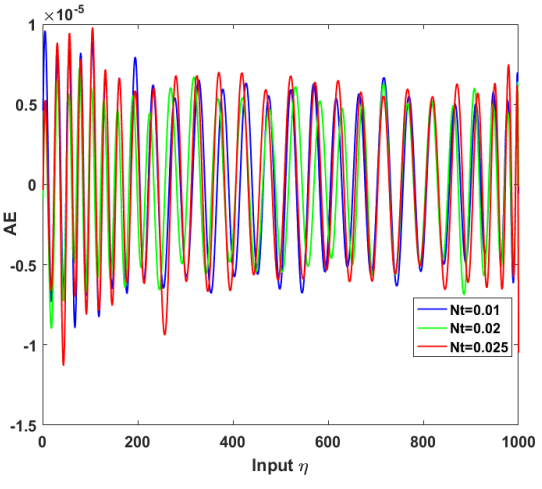

(f) AE evaluation

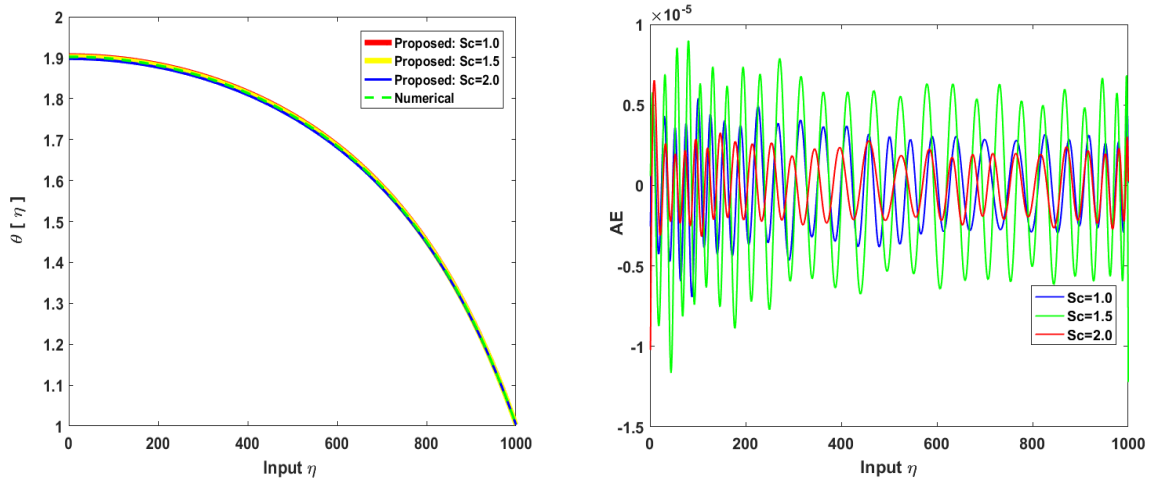

(g) Impact of Sc **(h) AE evaluation**

Figure 11. Comparison of the results of the proposed LMBNN model with those of the reference dataset under a uniform magnetic field for scenarios 4–7 is presented for the temperature profile θ[η], with Ec = 0.2, 0.3, 0.4; Nb = 1.0, 2.0, 3.0; Nt = 0.01, 0.02, 0.05 and Sc = 1.0, 1.5, 2.0.

6.1.1. Validation

The suggested BLMA-NN solver's validity was confirmed by contrasting it with analytical and numerical research that had already been published by Shateri et al. (J. Cent. South Univ., 2023). As shown, our model predicted a velocity drop of about 15.2% when the Hartmann number (Ha) was raised from 2 to 4, which is in close agreement with the ≈14.8% reported in the literature (deviation <0.5%). Likewise, the temperature rose by about 11% when the thermophoresis parameter (Nt) was doubled, which was in line with the trend of about 10.7% (error 0.3%). The BLMA-NN reproduces known physical behaviour and conforms with both analytical and published numerical results within 1-2% error, as further confirmed by regression values close to unity and fast convergence, guaranteeing accuracy and dependability.

The incredibly low MSE values in Table 3, which range from 10^{-11} to 10^{-12}, with convergence attained within 132–436 epochs and gradients as low as 3.1×10^{-8}, validate the accuracy of the suggested LMBNN solver. With only slight variations, the predicted velocity and temperature profiles closely resemble published numerical and analytical data, confirming the solver's resilience. This proves that the technique faithfully replicates the anticipated physical behaviour.

Table 3. Accuracy metrics of the proposed LMBNN solver, showing very low MSE, fast convergence, and small gradient values, confirming robustness and close agreement with published numerical and inalytical results.

MSE							
Training	**Validation**	**Testing**	**Execution**	**Gradient**	**Mu**	**Epoch**	**Time**
2.12E-11	2.31E-11	2.60E-11	2.00E-11	9.94E-08	E-11	159	12
4.80E-11	8.14E-11	5.57E-11	4.80E-11	9.97E-08	E-11	258	12
3.42E-11	3.83E-11	4.05E-11	3.40E-11	9.83E-08	E-12	132	9
1.24E-11	1.53E-11	1.41E-11	1.30E-11	9.99E-08	E-10	436	8
2.48E-12	1.38E-12	2.05E-12	2.50E-12	9.91E-08	E-11	166	11
2.80E-12	1.57E-12	1.05E-12	2.80E-12	3.10E-08	E-10	255	21
1.24E-11	1.53E-11	1.41E-11	1.40E-11	3.97E-08	E-10	1000	14

The characteristics listed earlier have real applications in several subdisciplines of physics; a summary follows. Composed of viscous media with suspended microstructures, micropolar fluids appear in different flow conditions and are distinguished by a nonsymmetric stress tensor. Essential in astrophysics, plasma physics, solar physics, and

biomedical applications such as magnetic drug delivery, tumor therapy, and blood flow control is magnetohydrodynamics (MHD), which studies how magnetic fields affect electrically conducting fluids. The relative thickness of the thermal and momentum boundary layers is determined by the Prandtl number: high-Pr fluids ($Pr > 1$, such as engine oil) promote convective heat transfer, whereas low-Pr fluids ($Pr < 1$, such as liquid mercury) favour conduction.

Brownian motion refers to the random movement of nanoparticles caused by molecular interactions, which plays a key role in stabilizing nanofluids by preventing particle sedimentation. This motion distinguishes colloidal solutions from true solutions. Under a temperature gradient, particles also migrate through thermophoresis, an effect important in high-temperature systems such as boilers and semiconductor processing, where it aids particle separation and impurity migration. Thermophoretic and electrostatic forces are also applied in commercial precipitators for particle control.

Vacuum deposition, commonly used for making optical fibers, also ensures cleanliness during transport. Thermophoresis is applied in drug development through microscale thermophoresis to detect aptamer binding, and in biophysics for localized heating to control macromolecules such as HIV particles and DNA in micro- and nanochannels. It is also used in field flow fractionation to separate polymer particles. The Lewis number defines the ratio of thermal to concentration boundary layer thickness, important in combined heat and mass transfer problems. Slip velocity, representing the average velocity of particles near solid boundaries, affects mass and heat transfer: higher mass transfer slip enhances mass transfer rates but reduces skin friction, heat transfer, and velocity profiles, while higher thermal slip slows both mass and heat transfer. In drilling operations, slip velocity influences particle settling and hole cleaning efficiency.

7. Conclusion

The suggested system uses Levenberg–Marquardt backpropagation neural network approaches to create a stochastic computing platform for fluid systems, including MHD nanofluids. The governing partial differential equations (PDEs) are transformed within the model into equivalent ordinary differential equations (ODEs), which correctly represent the dynamic behavior and flow characteristics of magnetohydrodynamic nanofluids. The dataset for the LMBNN method is created by Mathematica together with the RK4 numerical method, taking into account variations in important characteristics like Brownian movement, Lewis number, thermophoresis parameters, and Prandtl number. Utilizing 70% and 15% of the reference data, the neural network with 25 hidden neurons is trained, validated, and tested, respectively. The great consistency between the projected LMBNN results and reference solutions, which reach accuracy levels on the order of 10^{-11} to 10^{-12}, confirms the reliability of the method. Moreover, numerical and graphical studies, including error histograms, regression plots, and convergence curves based on the mean squared error (MSE) metric, show the technique's accuracy.

References

[1] B. Jalili, A. Rezaeian, P. Jalili, F. Ommi, D. D. Ganji, Numerical modeling of magnetic field impact on the thermal behavior of a microchannel heat sink, *Case Studies in Thermal Engineering,* Vol. 45, pp. 102944, 2023.

[2] P. Jalili, B. Jalili, A. Shateri, D. D. Ganji, A novel fractional analytical technique for the time-space fractional equations appearing in oil pollution, *Int. J. Eng,* Vol. 35, No. 12, pp. 2386-2394, 2022.

[3] B. Jalili, P. Jalili, A. Shateri, D. D. Ganji, Rigid plate submerged in a Newtonian fluid and fractional differential equation problems via Caputo fractional derivative, *Partial Differential Equations in Applied Mathematics,* Vol. 6, pp. 100452, 2022.

[4] A. Shafiq, T. Sindhu, Statistical study of hydromagnetic boundary layer flow of Williamson fluid regarding a radiative surface, *Results in Physics,* Vol. 7, pp. 3059-3067, 2017.

[5] T. Muhammad, T. Hayat, A. Alsaedi, A. Qayyum, Hydromagnetic unsteady squeezing flow of Jeffrey fluid between two parallel plates, *Chinese Journal of Physics,* Vol. 55, No. 4, pp. 1511-1522, 2017.

[6] P. Jalili, A. A. Azar, B. Jalili, Z. Asadi, D. D. Ganji, Heat transfer analysis in cylindrical polar system with magnetic field: a novel hybrid analytical and numerical technique, *Case Studies in Thermal Engineering,* Vol. 40, pp. 102524, 2022.

[7] P. S. Narayana, B. Venkateswarlu, B. Devika, Chemical reaction and heat source effects on MHD oscillatory flow in an irregular channel, *Ain Shams Engineering Journal,* Vol. 7, No. 4, pp. 1079-1088, 2016.

[8] S. Ahmad, F. Chishtie, A. Mahmood, Analytical technique for magnetohydrodynamic (MHD) fluid flow of a periodically accelerated plate with slippage, *European Journal of Mechanics-B/Fluids,* Vol. 65, pp. 192-198, 2017.

[9] K. Khanafer, K. Vafai, M. Lightstone, Buoyancy-driven heat transfer enhancement in a two-dimensional enclosure utilizing nanofluids, *International journal of heat and mass transfer,* Vol. 46, No. 19, pp. 3639-3653, 2003.

[10] S. U. Choi, J. A. Eastman, *Enhancing thermal conductivity of fluids with nanoparticles*, Argonne National Lab.(ANL), Argonne, IL (United States), pp. 1995.

[11] E. Abu-Nada, Z. Masoud, A. Hijazi, Natural convection heat transfer enhancement in horizontal concentric annuli using nanofluids, *International Communications in Heat and Mass Transfer,* Vol. 35, No. 5, pp. 657-665, 2008.

[12] N. S. Akbar, S. Nadeem, N. Noor, Free convective MHD peristaltic flow of a Jeffrey nanofluid with convective surface boundary condition: a biomedicine–Nano model, *Curr. Nanosci,* Vol. 10, No. 3, pp. 432-440, 2014.

[13] M. Turkyilmazoglu, A note on the correspondence between certain nanofluid flows and standard fluid flows, *Journal of Heat Transfer,* Vol. 137, No. 2, pp. 024501, 2015.

[14] M. Turkyilmazoglu, Flow of nanofluid plane wall jet and heat transfer, *European Journal of Mechanics-B/Fluids,* Vol. 59, pp. 18-24, 2016.

[15] R. Mohebbi, M. Rashidi, Numerical simulation of natural convection heat transfer of a nanofluid in an L-shaped enclosure with a heating obstacle, *Journal of the Taiwan Institute of Chemical Engineers,* Vol. 72, pp. 70-84, 2017.

[16] S. B. Abubakar, N. C. Sidik, Numerical prediction of laminar nanofluid flow in rectangular microchannel heat sink, *Journal of Advanced research in fluid mechanics and thermal sciences,* Vol. 7, No. 1, pp. 29-38, 2015.

[17] N. M. a. Muhammad, N. A. C. Sidik, Utilization of Nanofluids in Minichannel for Heat Transfer and Fluid Flow Augmentation: A Concise Research Design, *Journal of Advanced Research Design,* Vol. 50, No. 1, pp. 18-29, 2018.

[18] J. Buongiorno, Convective transport in nanofluids, 2006.

[19] D. Nield, A. Kuznetsov, The Cheng–Minkowycz problem for natural convective boundary-layer flow in a porous medium saturated by a nanofluid, *International journal of heat and mass transfer,* Vol. 52, No. 25-26, pp. 5792-5795, 2009.

[20] A. Kuznetsov, D. Nield, Natural convective boundary-layer flow of a nanofluid past a vertical plate, *International Journal of Thermal Sciences,* Vol. 49, No. 2, pp. 243-247, 2010.

[21] A. J. Chamkha, A. M. Rashad, C. RamReddy, P. Murthy, Viscous dissipation and magnetic field effects in a non-Darcy porous medium saturated with a nanofluid under convective boundary condition, *Special Topics & Reviews in Porous Media: An International Journal,* Vol. 5, No. 1, 2014.

[22] A. Hussain, M. Malik, T. Salahuddin, S. Bilal, M. Awais, Combined effects of viscous dissipation and Joule heating on MHD Sisko nanofluid over a stretching cylinder, *Journal of Molecular Liquids,* Vol. 231, pp. 341-352, 2017.

[23] W. Ibrahim, Magnetohydrodynamic (MHD) boundary layer stagnation point flow and heat transfer of a nanofluid past a stretching sheet with melting, *Propulsion and Power Research,* Vol. 6, No. 3, pp. 214-222, 2017.

[24] M. Rashidi, S. Abelman, N. F. Mehr, Entropy generation in steady MHD flow due to a rotating porous disk in a nanofluid, *International journal of Heat and Mass transfer,* Vol. 62, pp. 515-525, 2013.

[25] M. Sheikholeslami, S. Abelman, D. D. Ganji, Numerical simulation of MHD nanofluid flow and heat transfer considering viscous dissipation, *International Journal of Heat and Mass Transfer,* Vol. 79, pp. 212-222, 2014.

[26] M. Sheikholeslami, M. Gorji-Bandpy, D. Ganji, MHD free convection in an eccentric semi-annulus filled with nanofluid, *Journal of the Taiwan Institute of Chemical Engineers,* Vol. 45, No. 4, pp. 1204-1216, 2014.

[27] M. Sheikholeslami, D. Ganji, Heat transfer of Cu-water nanofluid flow between parallel plates, *Powder Technology,* Vol. 235, pp. 873-879, 2013.

[28] M. Sheikholeslami, D. D. Ganji, Ferrohydrodynamic and magnetohydrodynamic effects on ferrofluid flow and convective heat transfer, *Energy,* Vol. 75, pp. 400-410, 2014.

[29] M. Sheikholeslami, M. Gorji-Bandpy, D. D. Ganji, S. Soleimani, MHD natural convection in a nanofluid filled inclined enclosure with sinusoidal wall using CVFEM, *Neural Computing and Applications,* Vol. 24, No. 3, pp. 873-882, 2014.

[30] M. Hatami, D. Ganji, Heat transfer and nanofluid flow in suction and blowing process between parallel disks in presence of variable magnetic field, *Journal of Molecular Liquids,* Vol. 190, pp. 159-168, 2014.

[31] P. Jalili, H. Narimisa, B. Jalili, A. Shateri, D. Ganji, A novel analytical approach to micro-polar nanofluid thermal analysis in the presence of thermophoresis, Brownian motion and Hall currents, *Soft Computing,* Vol. 27, No. 2, pp. 677-689, 2023.

[32] D. Nield, A. V. Kuznetsov, Thermal instability in a porous medium layer saturated by a nanofluid, *International Journal of Heat and Mass Transfer,* Vol. 52, No. 25-26, pp. 5796-5801, 2009.

[33] M. Sheikholeslami, D. D. Ganji, M. Y. Javed, R. Ellahi, Effect of thermal radiation on magnetohydrodynamics nanofluid flow and heat transfer by means of two phase model, *Journal of magnetism and Magnetic materials,* Vol. 374, pp. 36-43, 2015.

[34] W. Khan, I. Pop, Boundary-layer flow of a nanofluid past a stretching sheet, *International journal of heat and mass transfer,* Vol. 53, No. 11-12, pp. 2477-2483, 2010.

[35] M. Sheikholeslami, D. Ganji, Nanofluid hydrothermal behavior in existence of Lorentz forces considering Joule heating effect, *Journal of Molecular Liquids,* Vol. 224, pp. 526-537, 2016.

[36] B. Manvi, J. Tawade, M. Biradar, S. Noeiaghdam, U. Fernandez-Gamiz, V. Govindan, The effects of MHD radiating and non-uniform heat source/sink with heating on the momentum and heat transfer of Eyring-Powell fluid over a stretching, *Results in Engineering,* Vol. 14, pp. 100435, 2022.

[37] V. M. Job, S. R. Gunakala, R. S. R. Gorla, O. Makinde, H. T. Basha, Unsteady convective ferrohydrodynamic flow of MnZnFe2O4/FeCrNbB-EG hybrid nanofluid in a horizontal channel with porous fins and semi-circular heaters, *Journal of Magnetism and Magnetic Materials,* Vol. 571, pp. 170584, 2023.

[38] M. Venkateswarlu, M. Prameela, O. Makinde, Influence of heat generation and viscous dissipation on hydromagnetic fully developed natural convection flow in a vertical micro-channel, *Journal of Nanofluids,* Vol. 8, No. 7, pp. 1506-1516, 2019.

[39] E. Oborin, H. Irschik, Application of a novel Picard-type time-integration technique to the linear and non-linear dynamics of mechanical structures: an exemplary study, *Applied Sciences,* Vol. 11, No. 9, pp. 3742, 2021.

[40] Z. Nasri, H. Binous, Rigorous distillation dynamics simulations using a computer algebra, *Computer Applications in Engineering Education,* Vol. 20, No. 2, pp. 193-202, 2012.

[41] H. Binous, A. Aheed, M. M. Hossain, Haber process and steam-coal gasification: Two standard thermodynamic problems elucidated using two distinct approaches, *Computer Applications in Engineering Education,* Vol. 24, No. 1, pp. 58-70, 2016.

[42] M. Umar, Z. Sabir, M. A. Z. Raja, J. G. Aguilar, F. Amin, M. Shoaib, Neuro-swarm intelligent computing paradigm for nonlinear HIV infection model with CD4+ T-cells, *Mathematics and Computers in Simulation,* Vol. 188, pp. 241-253, 2021.

[43] I. A.-H. Hassan, Application to differential transformation method for solving systems of differential equations, *Applied Mathematical Modelling,* Vol. 32, No. 12, pp. 2552-2559, 2008.

[44] A. Shateri, M. M. Moghaddam, B. Jalili, Y. Khan, P. Jalili, D. D. Ganji, Heat transfer analysis of unsteady nanofluid flow between moving parallel plates with magnetic field: analytical approach, *Journal of Central South University,* Vol. 30, No. 7, pp. 2313-2323, 2023.